ACS APPLIED MATERIALS & INTERFACES

Research Article

www.acsami.org

Room-Temperature Ferromagnetism in Thin Films of $LaMnO_3$ Deposited by a Chemical Method Over Large Areas

José Manuel Vila-Fungueiriño,[†] Beatriz Rivas-Murias,[†] Benito Rodríguez-González,[‡] O. Txoperena,[§] D. Ciudad,[§] Luis E. Hueso,[§] Massimo Lazzari,[†] and Francisco Rivadulla*[,†]

[†]Centro de Investigación en Química Biológica y Materiales Moleculares (CIQUS), Universidad de Santiago de Compostela, 15782 Santiago de Compostela, Spain

[‡]Departamento de Química Física, Universidad de Vigo, 36310 Vigo, Spain

[§]CIC-nanoGUNE and IKERBASQUE, Basque Foundation for Science, 20018 San Sebastian, Spain

Supporting Information

ABSTRACT: Hole-doping into the Mott insulator $LaMnO_3$ results in a very rich magneto-electric phase diagram, including colossal magneto-resistance and different types of charge and orbital ordering. On the other hand, $LaMnO_3$ presents an important catalytic activity for oxygen reduction, which is fundamental for increasing the efficiency of solid-oxide fuel cells and other energy-conversion devices. In this work, we report the chemical solution (water-based) synthesis of high-quality epitaxial thin films of $LaMnO_3$, free of defects at square-centimeter scales, and compatible with standard microfabrication techniques. The films show a robust ferromagnetic moment and large magnetoresistance at room temperature. Through a comparison with films grown by pulsed laser deposition, we show that the quasi-equilibrium growth conditions characteristic of this chemical process can be exploited to tune new functionalities of the material.

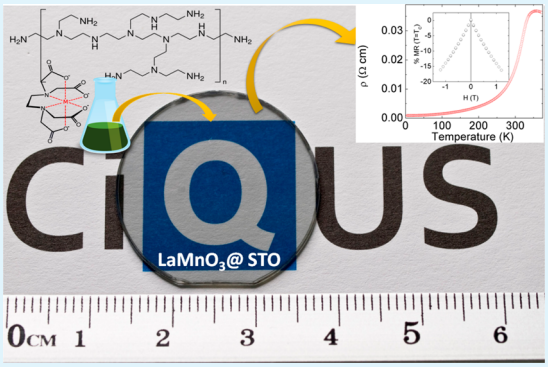

KEYWORDS: *polymer-assisted deposition, chemical solution deposition, thin-films, colossal magnetoresistance, manganites*

INTRODUCTION

Chemical methods for thin-film deposition are an affordable and versatile alternative to physical deposition techniques (pulsed laser deposition, sputtering, molecular beam epitaxy, etc.).[1−3] In particular, deposition from a solution is preferred to avoid the use of high-vacuum chambers, and, a priori, is suitable for coatings over large areas and complex-shaped objects.

Among the chemical methods based on a liquid precursor, spray deposition and sol−gel are the most widely used.[4] The first one involves the generation and deposition on a heated substrate of aerosols from the liquid bath. On the other hand, the sol−gel process requires the hydrolysis of organometallic salts to form a colloidal sol, condensation into a gel, and a subsequent thermal annealing to crystallize the inorganic film. An important advantage of this technique is that it is suitable for film deposition by spin and dip coating.[5]

However, in spite of the obvious advantages, chemical methods show some serious drawbacks when compared to physical deposition techniques: (1) poorer control of the thickness and stoichiometry, (2) larger interface and surface roughness; and resulting from these two, (3) difficult fabrication of homogeneous films and multilayers over large areas. Consequently, these problems limited the applicability of chemical deposition methods for the study of the subtle phenomena that occur at clean interfaces with a broken symmetry (spin, orbital, etc.),[6] or their use in highly demanding applications (tunnel junctions, etc.).[7]

In an important step forward in this direction, some of us recently demonstrated the possibility of fabricating hetero-epitaxial bilayers and functional tunnel junctions by a polymer assisted chemical deposition method (PAD).[8,9] This chemical method, originally introduced by Jia et al.,[10] was successfully applied to grow complex oxide films,[11−13] nitrides,[14,15] and carbides.[16]

In this study, we address the PAD synthesis of high quality epitaxial thin films of $LaMnO_3$, over large areas. This oxide is a Mott insulator which gives rise to a very rich electronic and magnetic phase diagram after hole doping, being the parent phase to colossal magnetoresistive oxides.[17] On the other hand, it has been recently identified as one of the most suitable catalysts for electrochemical oxygen reduction reactions[18] and for the oxidative removal of toluene.[19] Therefore, it will be very important the development of affordable techniques for deposition of $LaMnO_3$ thin films, with a large surface/volume ratio, and free of defects over large areas.

Received: December 20, 2014
Accepted: February 10, 2015
Published: February 10, 2015

DOI: 10.1021/am508941j
ACS Appl. Mater. Interfaces 2015, 7, 5410−5414

Here, we address for the first time all the relevant chemical aspects of the PAD process, to achieve homogeneous depositions of $LaMnO_3$ (below 20 nm thick) at cm^2 scales, compatible with standard microfabrication techniques, and very reproducible. We demonstrate that the quasi-equilibrium growth regime characteristic of this chemical method can be exploited, in conjunction with epitaxial strain, to tune the functionality of the material. Particularly, we show that a robust ferromagnetism and magnetoresistance can be induced at room temperature in thin films of $LaMnO_3$ synthesized by PAD.

EXPERIMENTAL SECTION

For the deposition of $LaMnO_3$ (LMO) thin films, individual solutions of La and Mn nitrates were dissolved in water with ethylenediaminetetraacetic acid (EDTA, 1:1 molar ratio), and polyethylenimine (PEI, 1:1 mass ratio to EDTA). The electrostatic interaction of the protonated amino groups of PEI with the $[EDTA\text{-}Metal]^{n-}$ complex is crucial for a successful deposition of an homogeneous film. PEI is a polymer in which primary, secondary, and tertiary amines with different pK_a, are present in different amounts depending on the degree of branching. Therefore, the pH, the degree of branching, molecular weight, and size distribution of polymeric molecules will play a very important role in this process. To make this a fully reproducible and scalable method, we performed a detailed characterization of the polymer and determined the influence of these parameters in the quality of the films. The degree of branching and molecular weight distribution of different commercial PEI was determined by ^{13}C, ^{1}H NMR and size exclusion chromatography. The thermal decomposition of the polymer was followed by thermogravimetric and IR analysis. A complete description of these analyses is given in the Supporting Information.

Very importantly, we have identified small polymeric fractions (≈ 5 kDalton) of highly branched structures, which present very different physical and chemical properties (particularly a much smaller solubility) to larger and less branched PEI molecules. These are present in all commercial PEI, due to the synthetic method used to prepare these polymers, and therefore it is imperative to remove them before spin-coating deposition, in order to avoid the formation of defects in the final film. Therefore, the solutions were purified by ultrafiltration using 10 kDalton filters, as detailed in the Supporting Information

Once purified, the individual solutions were mixed according to the desired final stoichiometry, and concentrated to ≈ 120 mM. The total cationic concentration of the solution determines the final thickness of the film, in a range from ≈ 4 nm (60 mM) to ≈ 30 nm (200 mM). The solutions were spin-coated on (001) $SrTiO_3$ (STO) substrates and annealed at 950 °C for 1h, in air.

RESULTS AND DISCUSSION

X-ray $2\theta-\omega$ scans of the LMO films present only the $(hh0)$ peaks in an extended range, confirming that all samples prepared in this work grow perfectly oriented with respect to the substrate (Figure 1). High-resolution reciprocal space mapping (RSM, Figure 1) and ϕ-scans (Supporting Information, Figure S12) confirm a perfect epitaxial matching.

Epitaxial growth was further investigated by high-resolution TEM in cross section lamellae prepared from the films. The results are shown in Figure 2a) for a thin film of LMO (18 nm thick) on STO. The films grow along the [110] direction, parallel to the [001] direction of the STO substrate, with a very smooth interface between the film and the substrate. This quality was observed for all the lamellae prepared, with an excellent homogeneity of the film over the whole substrate.

The comparison with a sample grown by pulsed laser deposition (PLD, Figure 2b), with the same nominal composition, shows that a similar crystalline quality and

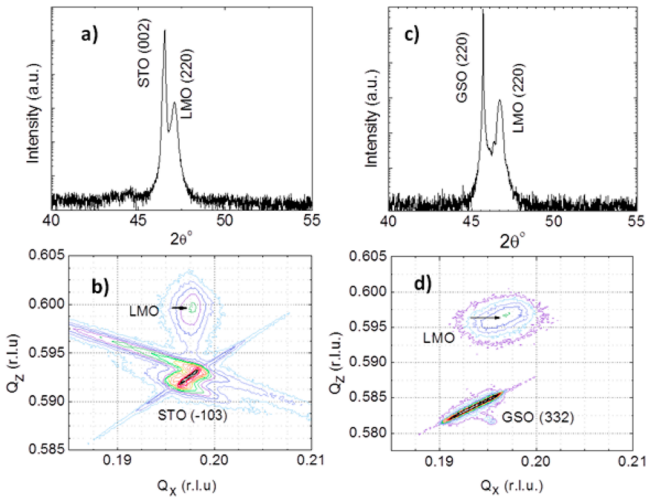

Figure 1. (a) X-ray $2\theta-\omega$ and (b) reciprocal space maps of $LaMnO_3$ thin films (≈ 18 nm) deposited on (001) STO by PAD. The orthorhombic (220) peak in the LMO film is equivalent to the (002) in the LMO pseudocubic setting. (c) X-ray $2\theta-\omega$ and (d) reciprocal space maps for identical films of $LaMnO_3$ deposited by PAD in $GdScO_3$ (110). In this case, the orthorhombic (332) peak is the equivalent to the pseudocubic $(\bar{1}03)$ in the (110) orientation.

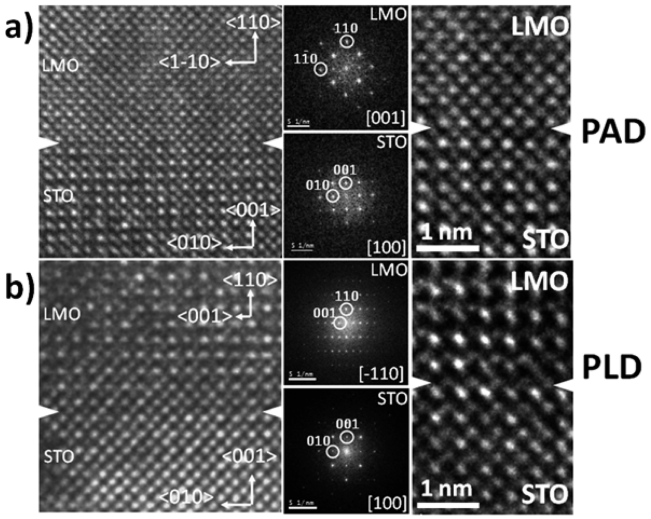

Figure 2. High-resolution cross-sectional TEM image of a $LaMnO_3$ film deposited on $SrTiO_3$ (001) by (a) PAD and (b) PLD. The growth direction is determined from the Fourier transform on each layer (middle panels).

interface roughness can be achieved by both methods. This is surprising, given their very different growth modes: the stoichiometric transfer of material from a target during PLD is characteristic of the nonequilibrium nature of the ablation process, and kinetic aspects are crucial during nucleation and growth of the crystalline film.[20] On the other hand, PAD implies a growth mode close to thermal equilibrium, and the material might find different ways of relaxing the stress imposed by epitaxial matching to the substrate. Therefore, important differences in the chemical and physical properties of a priori equivalent materials may be found depending on the growth technique.

$LaMnO_3$ is particularly suitable to study this possibility, as its structural and magnetoelectric properties are very sensitive to minute deformations of the lattice or chemical composition.

DOI: 10.1021/am508941j
ACS Appl. Mater. Interfaces 2015, 7, 5410−5414

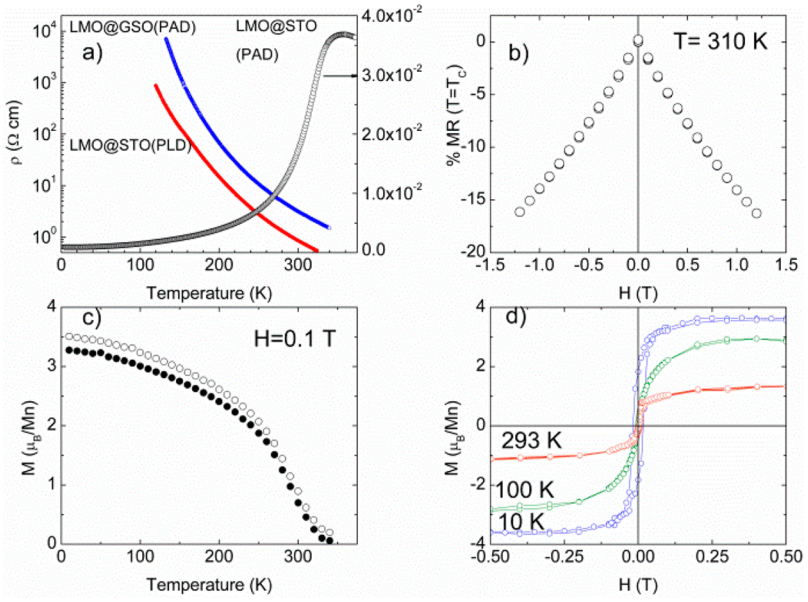

Figure 3. (a) Temperature dependence of the resistivity for a LMO film (≈ 18 nm) deposited on (001) STO by PAD. The resistivity for an identical film deposited in orthorhombic (110) $GdScO_3$ by PAD and for a film of LMO deposited in STO by PLD, are also shown. (b) Magnetoresistance at 310 K for the PAD film on STO shown in panel a. (c) Temperature and (d) field dependence of the magnetization for this film. The solid circles (●) in panel c show the result after a postannealing in O_2.

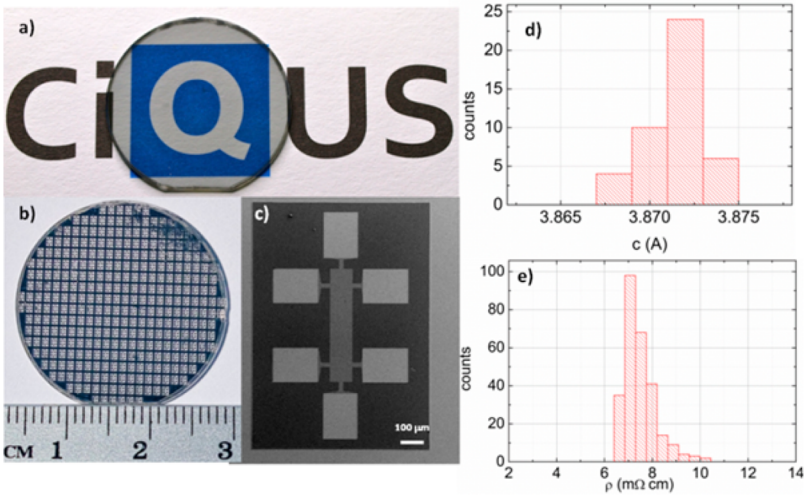

Figure 4. (a) Photograph of an 18 nm thick film of $LaMnO_3$, deposited by PAD on 1 in. diameter $SrTiO_3$ (001). (b) Photograph of the same film after patterning 324 Hall bars by photolithography and lift-off. (c) SEM image of a lithographed Hall bar. The dimensions of the channels are 100 × 500 μm. Distributions of (d) *c* axis lattice parameter and (e) electrical resistivity.

Bulk LMO is orthorhombic (*Pnma*, $a < b < c$), with a cooperative Jahn−Teller (JT) distortion that sets below $T_{JT} \approx 600$ °C. This stabilizes the d_z^2 orbital in the *ab* plane ($c/a < \sqrt{2}$, O′-*Pnma*), introducing a FM (AF) interaction in-plane (out-of-plane) which is the origin of the A-type AF structure in this compound.[21] The degree of orthorhombicity decreases very fast as Mn^{4+} replaces the JT active Mn^{3+} in LMO (through partial replacement of La^{3+} by Ca^{2+}, as in $La_{1-x}Ca_xMnO_3$, for example)[22] and the cell becomes pseudotetragonal for $x \geq 0.25$[23] (Figure S17 in the Supporting Information). Therefore, epitaxial growth of LMO on top of cubic STO introduces a strongly anisotropic compression in the *ab* plane. This is very expensive from an energetic point of view, as the tetragonal symmetry imposed by the substrate is incompatible with the in-plane ordering of d_z^2 orbitals. Therefore, a tendency to nucleate the nonstoichiometric $La_{1-x}MnO_3$ phase is expected to relax this stress if the film is grown in thermal equilibrium.

Indeed, EDX analysis show that the films deposited by PAD on (001) STO present a final composition La_xMnO_3, with $x \approx 0.92$, with spontaneous segregation of La_2O_3 (Figures S13 and S14, Supporting Information). An amount of La vacancies ≈ 8% is enough to introduce ≈ 24% of Mn^{4+} (holes) into the lattice and, hence, to destroy the cooperative static JT distortion. This severely reduces the orthorhombic distortion with respect to stoichiometric LMO, allowing an epitaxial growth without paying such a huge elastic energy penalty. These films are metallic and ferromagnetic at low temperatures, with magnetotransport properties similar to Ca-doped system but with a much higher Curie temperature and a metal insulator

DOI: 10.1021/am508941j
ACS Appl. Mater. Interfaces 2015, 7, 5410−5414

transition temperature $T_{MI} \approx 350$ K, resulting in a large magnetoresistive effect at room temperature (Figure 3).

The value of T_{MI} in La-deficient samples is particularly large, similar to that found in $La_{2/3}Sr_{1/3}MnO_3$, and much larger than in the stoichiometric Ca-doped systems.[17,24] This fact resembles the effect of a lower disorder at the A-site of the perovksite, with respect to the equivalent sample with ≈ 24% Ca.[25]

The effect of oxygen nonstoichiometry was studied by annealing the samples in flowing oxygen at 400 °C for 1 h. The effect over the Curie temperature and magnetic moment is very small (Figure 3c). Also, Mn vacancies should decrease the magnetic transition temperature.[26] Therefore, in this case the presence of oxygen and Mn vacancies do not seem relevant to explain the results.

We have also deposited thin films of LMO by PAD on $GdScO_3$ (110) substrates. These substrates are orthorhombic with pseudocubic in-plane lattice parameter $a = 3.973$ Å. Then, the effect of epitaxial stress induced in a layer of LMO should be negligible (Figure 1c,d). As expected from the previous discussion, we observed that in this case the films are stoichiometric, with transport properties similar to these prepared by PLD (Figure 3).

Note that PLD implies high-temperature deposition (typically around 850 °C), significantly larger than T_{JT}. Therefore, epitaxial growth of the stoichiometric phase will not be hampered by the lattice distortion imposed by the JT orbital ordering, and the samples are under compressive stress at room temperature and show semiconducting behavior (Figure 3) and $T_N = 150$ K, similar to the bulk (Supporting Information).

These results show that chemical methods could be exploited to access compositions and properties of the phase diagram of a given system difficult to reach by physical deposition methods. Therefore, both approaches are complementary for the synthesis of materials with new or improved functionalities.

Finally, to demonstrate the scalability of the method, we deposited a continuous, 18 nm thick conducting layer of LMO on a 1 in. substrate of (001) STO (Figure 4). Random X-ray diffraction experiments in 44 different areas (spot size, 150 μm^2) reveal a very narrow distribution of lattice parameters, $c = 3.871(2)$ Å, which demonstrate an extremely good crystalline homogeneity (Figure 4d). The lack of defects in this film was further corroborated by optical measurements (ellipsometry) in 35 different points uniformly distributed around the layer, also showing an exceptional homogeneity of the film over the whole area (Figure 5).

To demonstrate the electrical homogeneity, 324 Hall bars were fabricated on the 1 in. diameter wafer by conventional photolithography and consequent Ar^+ ion etching (Figure 4). A second photolithography process was done to define six contacts to each of the Hall bars, followed by sputtering of 50 nm of palladium (Pd) and lift-off in acetone. The results show that the room-temperature conductivity of all of them is in a very narrow range, $\rho = 7.48(6)$ mΩ cm (Figure 4e).

This degree of homogeneity over such a large area is extremely difficult (if possible) to achieve with conventional PLD or MBE deposition. The results are an important step forward for the fabrication of homogeneous films of this technologically important material by an affordable and environmentally friendly method.

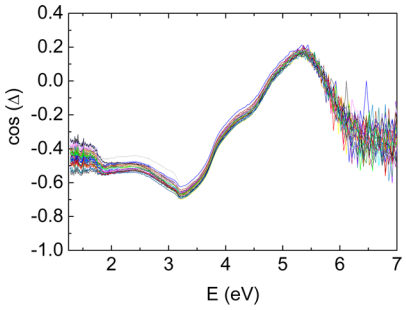

Figure 5. Ellipsometry measurements taken at 35 different points distributed in a square matrix uniformly covering the whole wafer. The measurements show little dispersion on composition and thickness, confirming the excellent homogeneity of the optical properties of the film.

CONCLUSIONS

We have demonstrated that, after a careful optimization of the relevant parameters, epitaxial thin films of multication oxides can be deposited with an exceptional morphological, structural, chemical, and electronic homogeneity over large areas and compatibility with the requirements of standard microfabrication techniques. Moreover, the growth regime of this chemical method can be exploited to add further functionalities to the deposited material because it is complementary to physical deposition techniques.

ASSOCIATED CONTENT

Supporting Information

Details of the preparation of the solutions, complete characterization of the polymers, and structural and transport data of the films. This material is available free of charge via the Internet at http://pubs.acs.org.

AUTHOR INFORMATION

Corresponding Author

*E-mail: f.rivadulla@usc.es.

Notes

The authors declare no competing financial interest.

ACKNOWLEDGMENTS

The authors thank Dr. M. Bañobre from INL (Portugal) and Dr. Sarah Fiol and Dr. Juan Antelo from USC for their help in the viscosity measurements and potentiometric titrations, respectively. This research was supported by the European Research Council (ERC StG-2DTHERMS; ERC StG-SPINTROS), Ministerio de Economía y Competitividad of Spain (MAT2013-44673-R and MAT2012-37638, and Xunta de Galicia (2012-CP071). J.M.V.-F and O.T. also acknowledge MINECO for support with a Ph.D. grant of the FPI program.

REFERENCES

(1) Valeri, S.; Benedetti, S. In *Oxide Ultrathin Films: Science and Technology*; Pacchioni, G., Valeri, S., Eds.; Wiley-VCH: Weinheim, 2012; Chapter 1.

(2) Sounart, T. L.; Liu, J.; Voigt, J. A.; Hsu, J. W. P.; D. Spoerke, E.; Tian, Z.; Jiang, Y. B. Sequential Nucleation and Growth of Complex Nanostructured Films. *Adv. Funct. Mater.* **2006**, *16*, 335−344.

(3) Wang, H.; He, Q.; Wang, H.; Wang, X.; Zhang, J.; Jiang, Y.; Li, Q. Intrinsic Room Temperature Ferromagnetism in $Zn_{0.92}Co_{0.08}O$ Thin Films Preprared by Pulsed Laser Deposition. *Thin Solid Films* **2011**, *519*, 3312−3317.

DOI: 10.1021/am508941j
ACS Appl. Mater. Interfaces 2015, 7, 5410−5414

(4) *Chemical Solution Deposition of Functional Oxide Thin Films*; Schneller, T.; Waser, R.; Kosec, M.; Payne, D., Eds.; Springer-Verlag: Wien, 2013.
(5) Brinker, C. J.; Frye, G. C.; Hurd, A. J.; Ashley, C. S. Fundamentals of Sol−Gel Dip Coating. *Thin Solid Films* **1991**, *201*, 97−108.
(6) Hwang, H. Y.; Iwasa, Y.; Kawasaki, M.; Keimer, B.; Nagaosa, N.; Tokura, Y. Emergent Phenomena at Oxide Interfaces. *Nat. Mater.* **2012**, *11*, 103−112.
(7) Harada, T.; Ohkubo, I.; Lippmaa, M.; Sakurai, Y.; Matsumoto, Y.; Muto, S.; Koinuma, H.; Oshima, M. Large Tunnel Magnetoresistance in Epitaxial Oxide Spin-Filter Tunnel Junctions. *Adv. Funct. Mater.* **2012**, *22*, 4471−4475.
(8) Vila-Fungueiriño, J. M.; Rivas-Murias, B.; Rodríguez-González, B.; Rivadulla, F. Interface Magnetic Coupling in Epitaxial Bilayers of $La_{0.92}MnO_3/LaCoO_3$ Prepared by Polymer-Assisted Deposition. *Chem. Mater.* **2014**, *26*, 1480−1484.
(9) Lucas, I.; Vila-Fungueiriño, J. M.; Jiménez-Cavero, P.; Rivas-Murias, B.; Magén, C.; Morellón, L.; Rivadulla, F. Tunnel Conduction in Epitaxial Bilayers of Ferromagnetic $LaCoO_3/La_{2/3}Sr_{1/3}MnO_3$ Deposited by a Chemical Solution Method. *ACS Appl. Mater. Interfaces* **2014**, *6*, 21279.
(10) Jia, Q. X.; McCleskey, T. M.; Burrell, A. K.; Lin, Y.; Collis, G. E.; Wang, H.; Li, A. D. Q.; Foltyn, S. R. Polymer Assisted Deposition of Metal-Oxide Thin Films. *Nat. Mater.* **2004**, *3*, 529−532.
(11) Zou, G.; Luo, H.; Zhang, Y. Y.; Xiong, J.; Wei, Q. M.; Zhuo, M. J.; Zhai, J. Y.; Wang, H. Y.; Williams, D.; Li, N.; Bauer, E.; Zhang, X. H.; McCleskey, T. M.; Li, Y. R.; Burrell, A. K.; Jia, Q. X. A Chemical Solution Approach for Superconducting and Hard Epitaxial NbC Film. *Chem. Commun.* **2010**, *46*, 7837−7839.
(12) Rivadulla, F.; Bi, Z.; Bauer, E.; Rivas-Murias, B.; Vila-Fungueiriño, J. M.; Jia, Q. X. Strain-Induced Ferromagnetism and Magnetoresistance in Epitaxial Thin Films of $LaCoO_3$ Prepared by Polymer-Assisted Deposition. *Chem. Mater.* **2013**, *25*, 55−58.
(13) Burrell, A. K.; McCleskey, T. M.; Jia, Q. X. Polymer Assisted Deposition. *Chem. Commun.* **2008**, 1271−1277.
(14) Luo, H.; Lin, Y.; Wang, H.; Lee, J. H.; Suvorova, N. A.; Mueller, A. H.; Burrell, A. K.; McCleskey, T. M.; Bauer, E.; Usov, I. O.; Hawley, M. E.; Holesinger, T. G.; Jia, Q. X. A Chemical Solution Approach to Epitaxial Metal Nitride Thin Films. *Adv. Mater.* **2009**, *21*, 193−197.
(15) Luo, H.; Wang, H.; Zou, G.; Bauer, E.; McCleskey, T. M.; Burrell, A. K.; Jia, Q. X. A Review of Epitaxial Metal-Nitride Films by Polymer Assisted Deposition. *Trans. Elect. Elect. Mater.* **2010**, *11*, 54−56.
(16) Zou, G.; Wang, H.; Mara, N.; Luo, H.; Li, N.; Di, Z.; Bauer, E.; Wang, Y.; McCleskey, T. M.; Burrell, A. K.; Zhang, X. H.; Nastasi, M.; Jia, Q. X. Chemical Solution Deposition of Epitaxial Carbide Films. *J. Am. Chem. Soc.* **2010**, *132*, 2516−2517.
(17) Imada, M.; Fujimori, A.; Tokura, Y. Metal-Insulator Transitions. *Rev. Mod. Phys.* **1998**, *70*, 1039−1263.
(18) Suntivich, J.; Gasteiger, H. A.; Yabuuchi, N.; Nakanishi, H.; Goodenough, J. B.; Shao-Horn, Y. Design Principles for Oxygen Reduction Activity on Perovskite Oxide Catalysts for Fuel Cells and Metal-Air Batteries. *Nat. Chem.* **2011**, *3*, 546−550.
(19) Wang, Y.; Xie, S.; Deng, J.; Deng, S.; Wang, H.; Yan, H.; Dai, H. Morphologically Controlled Synthesis of Porous Spherical and Cubic $LaMnO_3$ with High Activity for the Catalytic Removal of Toluene. *ACS Appl. Mater. Interfaces* **2014**, *6*, 17394−17401.
(20) *Pulsed Laser Deposition of Thin Films*; Eason, R., Ed.; John Wiley & Sons: Hoboken, NJ, 2007.
(21) Goodenough, J. B.; *Magnetism and the Chemical Bond*;. Interscience Publishers: New York, 1963.
(22) Hwang, H. Y.; Cheong, S.-W.; Radaelli, P. G.; Marezio, M.; Batlogg, B. Lattice Effects on the Magnetoresistance in Doped $LaMnO_3$. *Phys. Rev. Lett.* **1995**, *75*, 914−917.
(23) Radaelli, P. G.; Marezio, M.; Hwang, H. Y.; Cheong, S.-W.; Batlogg, B. Charge Localization by Static and Dynamic Distortions of the MnO_6 Octahedra in Perovskite Manganites. *Phys. Rev. B* **1996**, *54*, 8992−8995.
(24) Gupta, A.; McGuire, T. R.; Duncombe, P. R.; Rupp, M.; Sun, J. Z.; Gallgher, W. J.; Xiao, G. Growth and Giant Magnetoresistance Properties of La-Deficient $La_xMnO_{3-\delta}$ ($0.67 < x < 1$) films. *Appl. Phys. Lett.* **1995**, *67*, 3494−3496.
(25) Rodríguez-Martínez, L. M.; Attfield, J. P. Cation Disorder and Size Effects in Magnetoresistive Manganese Oxide Perovskites. *Phys. Rev. B* **1996**, *54*, R15622−15625.
(26) Horyn, R.; Zaleski, A. J.; Bukowska, E.; Sikora, A. On Magnetic Properties of $LaMnO_{3\pm\delta}$ Phase Within its Domain. *J. Alloys Comp.* **2004**, *383*, 80−84.

DOI: 10.1021/am508941j
ACS Appl. Mater. Interfaces 2015, 7, 5410−5414